ORIGINAL PAPER

Experimental and numerical investigation of centric and eccentric footing in reinforced sandy soil slope

Emel Turker[1] · Evrim Cure[1]

Abstract

This paper presents the findings regarding the displacement-load behavior of both plane strain model experiments' ultimate load and numerical analyses conducted on unreinforced and reinforced sand slopes loaded with strip footing. The investigated parameters include the impact of the reinforcement and varying eccentricity on the ultimate load and displacement of the strip footing. A group of finite element analyses was performed with the 3D plane strain model and the computer code ANSYS software to validate the results of the model experiments on a slope. The results from both the numerical analyses and model experiments suggested that the use of reinforcement could enhance the load–displacement behavior of the central and eccentrically loaded footings. The load–displacement curves demonstrated that a higher load eccentricity leads to a reduction in the ultimate load of the strip footing. The concordance between the computed and observed results was reasonably satisfactory for the load displacement and the overall behavioral trend.

Keywords Sandy soil slope · Footing · Reinforcement · Load–displacement behavior · Numerical simulation

Introduction

The bearing capacity is one of the main problems in foundation engineering. Footings were used to determine the number of engineered structures. These structures can transfer centric or eccentric loads to their footings. The eccentricity (e) in a strip footing is obtained by dividing the moment (M) by the vertical load (Q). A moment occurs as a result of horizontal loads affecting the structure. Currently, nearly all foundations are influenced by moments because of the horizontal loads affecting the structures. In recent years, different types of structures have been constructed on and near slopes. Owing to both the presence of a slope and eccentricity, the length of one of the failure surfaces was shorter. Therefore, the bearing capacity of the footing on or near the slope decreased compared to the foundation on horizontal flat soil.

The bearing capacities of foundations on horizontal flat soils have been extensively investigated by numerous researchers over the years using analytical, experimental, and numerical methods (Eastwood 1955; Chummar 1972; Ko and Davidson 1973; Pfeifle and Das 1979; Nova and Montrasio 1991; Andrawes et al. 1996; Briaud and Gibbens 1999; Taiebat and Carter 2000; Lau and Bolton 2011; Dixit and Patil 2013; Badakhshan and Noorzad 2015; Ahad and Arsam 2018; Khan and Sharma 2023; etc.). In addition, the failure surfaces of foundation soil have been researched in some of these studies (Binquet and Lee 1975a, b; etc.). However, studies on foundations situated on or near slopes are considerably restricted. The presence of a slope significantly affects the bearing capacity of footings of diverse structures. Designing footings under these circumstances is intricate, and the literature lacks sufficient information (Al-Jubair and Abbas 2007; Castelli and Motta 2010; Abbas and Sabbar 2011; Castelli and Lentini 2012; Keskin and Laman 2013; Munawir et al. 2013; Taha and Altalhe 2013; Cure et al. 2014a, b; Cure et al. 2014a, b; Turker et al. 2014; etc.).

Consequently, researchers have focused on investigating alternative ways to enhance the bearing capacity of soils on slopes (Selvadurai and Gnanendran 1989; Huang et al. 1994;

✉ Emel Turker
emelturker@ktu.edu.tr

Evrim Cure
evrimcure@ktu.edu.tr

[1]   Department of Civil Engineering, Karadeniz Technical University, 61080 Trabzon, , Türkiye

Lee and Manjunath 2000; Yoo 2001; Blatz and Bathurst 2003; Bathurst et al. 2003; Sawwaf 2007; Thanapalasingam and Gnanendran 2008; Alamshahi and Hataf 2009; Choudhary et al. 2010; Altalhe et al. 2013; Mehdipour et al. 2013; Ahmadi and Asakereh 2015; Altalhe et al. 2015; Xiao et al. 2019; Yang et al. 2021; Aliyazicioglu et al. 2023; Luo, et al. 2023; Mase et al. 2023; etc.).

Over the last five decades, geosynthetics have been utilized in soils to improve the bearing capacity. This is achieved by horizontally positioning geosynthetic sheets with vertical spacing beneath the footing by integrating the clippings of geosynthetics into the soil. Evidently, geosynthetics result in an augmented soil bearing capacity.

The aim of this research is to examine the displacement and bearing capacity characteristics of strip footings positioned under eccentric loads near unreinforced and

reinforced sand slopes. Additionally, numerical analysis was conducted on a prototype foundation-slope system using ANSYS (professional version v.10) to validate the finite element results with the existing model test outcomes. The advantage of developing a finite element model lies in its ability to explore different conditions that are not easily modeled in experimental studies. Furthermore, the scaling and size effects of the small-scale model tests were assessed using finite element analysis. The failure modes producing the ultimate bearing capacity and displacement were discussed by comparing the model tests and analysis results.

Experimental study

Test equipment

The components of the experimental design for the model tests consisted of a tank with internal dimensions, as shown in Fig. 1, sand, geotextile, strip footing, and loading system. Figures 1 and 2 show the general schematic of the experimental design.

The tank was rigid, such that the plane strain cases remained the same in all model tests. There are two primary cases for the plane-strain condition. In the first case, the displacement in the lateral direction must be zero ($\varepsilon_y = 0 = \Delta W/W$, where ε_y represents the displacement in the lateral direction, ΔW signifies the lateral displacement of the side faces of the tank, and W denotes the tank width). This requirement indicates the necessity for rigid front and back faces in plane-strain models. In the second case, the
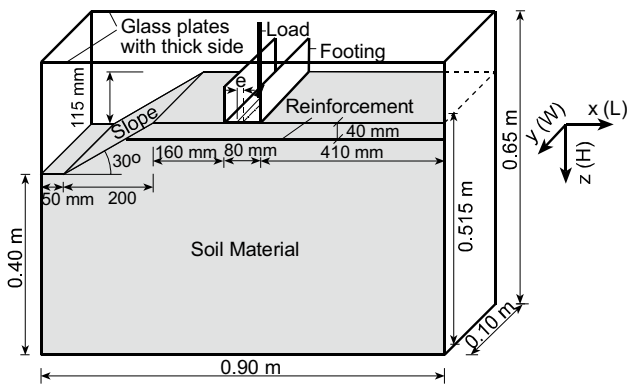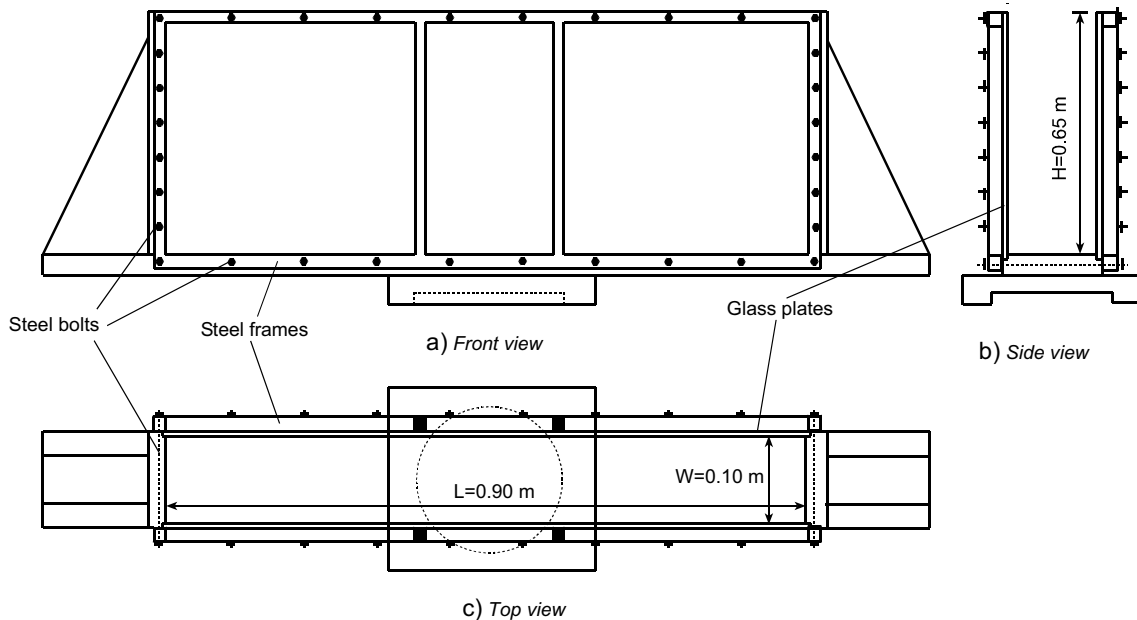

Fig. 1 View of the experimental design

Fig. 2 The tank's three views

friction between the tank's inner front and back faces and the soil must be zero, indicating completely frictionless inner surfaces. Although these ideal conditions cannot be fully realized in models, some criteria need to be met. Failure to do so could result in significant errors in the experimental outcomes, failing to represent a case of plane strain (Ko and Davidson 1973; Kirkpatrick and Yanikian 1975).

To ensure plane strain conditions, two steel frames made of hollow profiles were fabricated and interconnected along their edges using steel bolts. Solid steel elements were welded within the center of the frames to safeguard against deformation of the glass plates. The surface where the steel frames contacted the glass plates was meticulously crafted to a near-perfect plane, ensuring that no glass plate broke during the tests. The base and sides of the tank were constructed with rigid wood. For test preparation, the front and back surfaces were made of glass plates, 20-mm thick, allowing observation of the filling of the sand sample, deformation of sand particles during tests, and examination of fracture surfaces.

A loading system that allows the application of a vertical load on small-scale footing models was used (Fig. 3). The load was exerted on the model footing using a hydraulic jack with a capacity of 10 kN. A constant loading rate of 0.15 mm/min was selected and administered using a triaxial
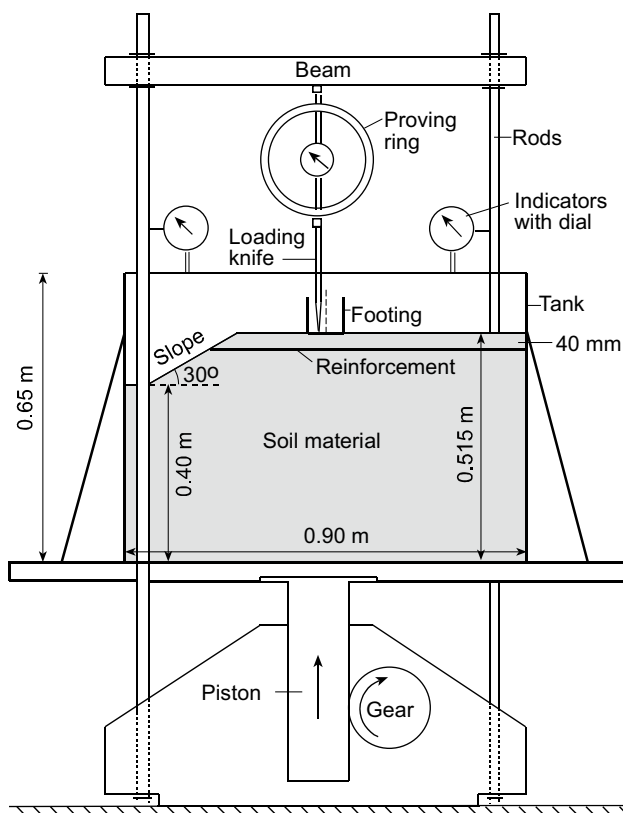
test apparatus. The tank was positioned atop the triaxial piston head, which had a rounded socket.

The loading tests utilized a strip footing with a width of 80 mm, length of 100 mm, and height of 80 mm, constructed by 8-mm-thick steel plates to ensure rigidity (Fig. 4). To achieve full frictional conditions along its base, the underside of the footing was roughened by applying coarse sandpaper. Grooves with V-shaped were carved along the base plate's length, allowing for various eccentricities ($e/B = 0$, $e/B = 1/12 = 6.7$ mm, $e/B = 1/6 = 13.3$ mm, and $e/B = 1/3 = 26.7$ mm). To prevent possible changes in the eccentricity of the rotating footing during the tests, a thickness of 2 mm was applied under the grooves.

Plane strain conditions were achieved by setting the length of the foundation, which was placed directly on the sand surface, equal to the width of the tank.

The load was applied using a sharp edge of the loading knife positioned on specific grooves based on eccentricity. This load was supported through a 6 kN capacity proving ring attached to the upper beam of the press. The elevation of the tank was gauged by affixing two indicators dial to the side rods of the press. The calculation of the footing's vertical displacement involved subtracting the deformation of the load ring from the tank's average height during the test. Additionally, two dial indicators positioned on the glass plates were employed to determine the lateral deformation of the glass plates.

Test materials

The fill soil utilized for the model tests in this research was locally sourced Black Sea Coastal Sand, characterized by a particle size distribution spanning approximately 0.2 to 4 mm (medium-coarse). According to the Unified Soil Classification System (USCS), this fill soil was categorized as poorly graded (*SP*) (ASTM D-6913, 2017). Table 1 outlines the physical properties of the sand.
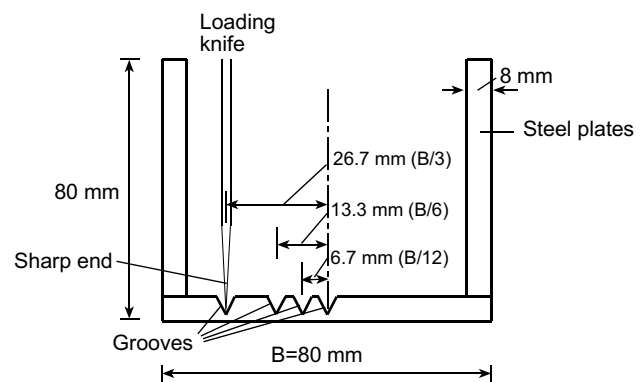

Fig. 3 The experimental design's loading mechanism

Fig. 4 View of the strip footing

Table 1 The sand's physical properties

Physical property	Symbol	Unit	Quantity
Effective diameter	D_{10}	mm	0.58
Diameter corresponding to 30% passing percentage	D_{30}	mm	0.80
Diameter corresponding to 60% passing percentage	D_{60}	mm	0.95
Curvature coefficient	C_r	-	1.16
Uniformity coefficient	C_u	-	1.64
Particle specific density (ASTM D854-14)	G_s	-	2.66
Internal friction angle (ASTM D3080/D3080M-11)	$\phi_{direct\ shear}$	degree	41
Internal friction angle (ASTM D7181-20)	$\phi_{triaxial}$	degree	43
Dry density	ρ_{dry}	Mg/m^3	1.581
Minimum dry density (ASTM D4254-16)	$\rho_{dry(min)}$	Mg/m^3	1.395
Maximum dry density (ASTM D4253-16)	$\rho_{dry(max)}$	Mg/m^3	1.658

At a relative density of $D_r = 0.74$, the internal friction angles of the sand were determined using shear box tests with internal dimensions of 60 mm × 60 mm, and triaxial tests with a diameter of $D = 38$ mm. A study by Cornforth in 1964 suggested a relationship among ϕ_{sb} shear box (sb), ϕ_{tr} triaxial (tr), and ϕ_{ps} (plane strain) angles.

$$\phi_{sb} < \phi_{tr} < \phi_{ps} \tag{1}$$

The difference between these calculated angles can reach up to 8 degrees.

At a relative density of $D_r = 0.74$, the internal friction angles of the sand were 41° (ϕ_{sb}) in the shear box tests and 43° (ϕ_{tr}) in the triaxial tests (Table 1). For strip footings, it is necessary to calculate the ideal internal friction angle from the plane strain (ϕ_{ps}). As determining the sand's internal friction angle calculated from the plane strain (ϕ_{ps}) experimentally was not feasible, according to the Lade and Lee (1976) formula, it was presumed to be 48°.

$$\phi_{ps} = 1.5\phi_{tr} - 17°(\phi_{tr} > 34°) \tag{2}$$

To achieve a general shear failure during the tests, the sand was positioned within the tank at an appropriate density, consistently maintaining a relative density of $D_r = 0.74$ throughout all the tests. In the tests, the sand was layered in 50-mm increments to create a flat height of 400 mm and a slope height of 115 mm within the tank (Fig. 3). Each 50-mm layer (7112 g) was loosely deposited as a uniform layer approximately 57-mm thick and lightly compacted to reach a thickness of 50 mm using a wooden hammer. Horizontal lines were drawn at intervals of 50 mm on the internal face of the glass plate to ensure thickness of the layer. This process was performed until the sand measured 0.4 m (5B) in height. For a slope height of 115 mm, three wooden wedges were used to build the layers gradually. Initially, a wooden wedge was positioned on a flat soil mass with a height of 400 mm, and 6382 g of sand was added to form a thick layer of 50 mm in the tank. Subsequently, a second wooden wedge was positioned atop the first one, and 2852 g of sand was deposited to create a 25-mm layer. This was followed by positioning a geotextile and adding an additional 2852 g of sand to form another 25-mm-thick layer. Finally, the procedure was replicated for a 15-mm-thick layer. Once the sand-filling process was completed, a model footing with a width of 80 mm was positioned. Considering the common practice of taking a significant depth (usually (3–4) times the footing width) for strip foundations, sand with a depth of 0.515 m beneath the footing was deemed adequate, as it represents the most influential depth. The dry or relative density of the sand in the tank was determined by measuring the mass of the removed sand. Prior to the actual tests, multiple sand fillings were conducted in the tank, demonstrating strong concordance among the trials. The relative density error was < 1% in these instances. Utilizing this sand-filling method in the tank eliminates the necessity for excavation and facilitates the creation of a sloping surface with a desired angle, thereby enabling uniform sand compaction. Subsequently, the strip footing was positioned on top of the compacted sand, and the load was incrementally applied until failure occurred.

A geotextile made of woven polypropylene, provided by Salteks Ltd., Istanbul, Türkiye, was used as reinforcement within the sand fill at a depth of 40 mm (B/2) for each trial. The reinforcement was placed horizontally behind the slope face along the length of the slope and across the footing direction (from the boundary of the tank to the sloped fill surface). The geotextile properties are listed in Table 2.

Test procedure

The tank was positioned on the piston and filled with sand. Selvadurai and Gnanendran (1989) and Laman et al. (2007) identified the optimal depth of the geotextile as B/2 for maximum effectiveness. Hence, in this study, a sole woven geotextile matching the tank plan area was horizontally embedded beneath the surface of the sand at a depth of

Table 2 The geotextile properties

Property	Unit	Quantity
Width of roll	m	5.2
Mass per unit area	g/m^2	430
Modulus of initial tangent	kN/m	218.9
Tensile strength (longitudinal-transverse)	kN/m	86
Elongation at break (longitudinal-transverse)	%	14

$B/2 = 40$ mm. Subsequently, at a distance of 160 mm ($D_e = 2$ B) from the edge of the slope, the footing was positioned as depicted in Fig. 3. The upper beam was set in place and the loading mechanism descended onto the sand. Two dial indicators were attached to the glass walls, and two dial indicators were affixed to the piston rods. Gradual load increments were applied until failure occurred, and at consistent time intervals, data collected from indicators with a dial were documented. The footing displacements, lateral deformations of the glass walls, and applied loads were measured using all indicators with a dial. When a failure occurred, the test was stopped.

Test program

The primary focus of the test program involved conducting load tests on a strip footing positioned on both unreinforced and reinforced slopes. Experiments performed at different eccentricities were replicated several times to validate the reliability and consistency of the collected data. Load–displacement curves were obtained for the test models, and the ultimate bearing loads were determined from the response curves.

Numerical modeling

This study employed ANSYS (professional version v.10), utilizing the finite element method, to analyze the behaviors exhibited by both unreinforced and reinforced sand slopes. ANSYS offers a broad spectrum of finite element analysis capabilities, encompassing simple linear static analyses to intricate nonlinear transient dynamic analyses and rendering effective solutions for numerous geotechnical engineering problems.

In the ANSYS program, eight nodded solid elements (SOLID 185) suitable for solid-volume elements were chosen. SOLID 185 was employed for the three-dimensional modeling of solid structures, characterized by eight nodes, each possessing three degrees of freedom.

When geometric modeling was performed, the wooden sides in the test tank and the outer surfaces of the glass plates were considered rigid. To solve the contact problem, contact elements were created with 0.1-mm spacing between the
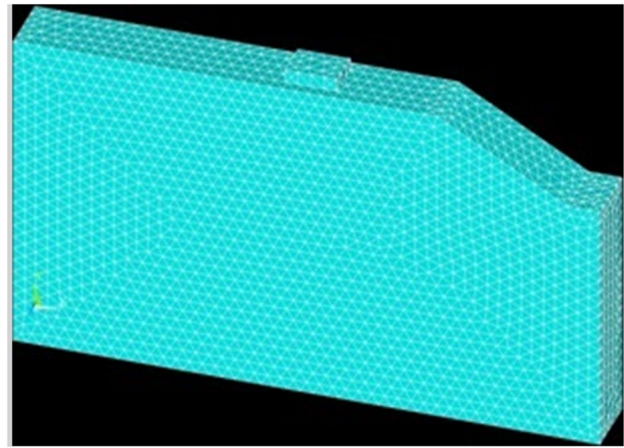
Fig. 5 Solid mesh of soil and footing modeling

glass and sand surfaces. Glass surfaces and steel model strip footing were defined as linear-elastic materials, whereas the behavior of sand was used as the Drucker–Prager model. The friction angle between the glass and sand surfaces was set as 11°. It was assumed that there was full friction between the sand and model footing. The friction angle between the sand and model footing was accepted as 40° because this value was close to the internal friction angle (Kumar and Bhoi 2008).

Soil modeling

In this study, the soil was considered as sand with dimensions of 900 mm × 100 mm × 500 mm, modulus of elasticity of 24,000 kN/m^2, Poisson's ratio of 0.2, dry density of 1.581 Mg/m^3, cohesion of 0.005 N/mm^2, and internal friction angle of 41°. The behavior of the soil, acting as an elastic-perfectly plastic material, was simulated using the Drucker-Prager yield criterion to replicate sand characteristics. The sand-soil model is shown in Fig. 5.

Geosynthetic reinforcement modeling

In this study, the geotextile served as a type of reinforcement to enhance the bearing capacity. The selection of the structural element to replicate the soil reinforcement and its interaction with the soil is of substantial importance for numerical modeling outcomes (Yu et al. 2015). The dimensions of the reinforcement were 770 mm × 100 mm. Reinforcement modeling utilized the Linear Isotropic Model as its material representation and employed link 8 as the element type.

Strip footing modeling

In this study, the strip footing was modeled as steel, using a Linear Isotropic Model as the material and Solid 45 as

the element type. The dimensions of the steel footing were 80 mm × 100 mm × 8 mm. The input data for this model was a modulus of elasticity of 200×10^6 kN/m^2 and Poisson's ratio of 0.3. The model footing had coarse sandpaper affixed to its base, ensuring a complete boundary at the interface.

Figure 5 shows the finite element mesh of a sand slope subjected to axially vertically loaded strip footing. The dimensions of the numerical model for plane strain were identical to those of the experimental setup. In the model, the lower boundary constrained both horizontal and vertical deformations, whereas only the horizontal deformation was constrained in the lateral boundaries. This approach aims to replicate the boundary conditions of the experimental design as closely as possible.

Results and discussions

Tests on bearing capacity were conducted by employing strip footing subjected to eccentric loading in proximity to both unreinforced and reinforced sand slopes. The tests were conducted using eccentricities ranging from $e/B = 0$ to $1/3$ on dense sand at a relative density (D_r) of 0.74. Experiments performed at different eccentricities were replicated twice to ensure accuracy of the experimental measurements. Therefore, this study focused on determining and assessing the impact of eccentricity on the ultimate load–displacement behavior. In addition, a numerical analysis of a prototype footing-slope system based on an experimental design was conducted to examine the impact of the same parameter. The analysis was performed using the finite element program ANSYS (professional version v.10). The sand was simulated using an elastic-perfectly plastic material model. The program's validation involved comparing the experimental research findings with those obtained from the numerical analysis.

Load–displacement relations

Unreinforced case

Figures 6, 7, 8 and 9 present the comparison between the load–displacement relations calculated using finite element analyses and results obtained from the model tests for the strip footing subjected to central and eccentrical loading, positioned near unreinforced sand slope. The figures show that the model test results corroborate the findings obtained through finite element analysis, and the load–displacement relation of model test shows similarity with the load–displacement relation of finite element analysis. The difference
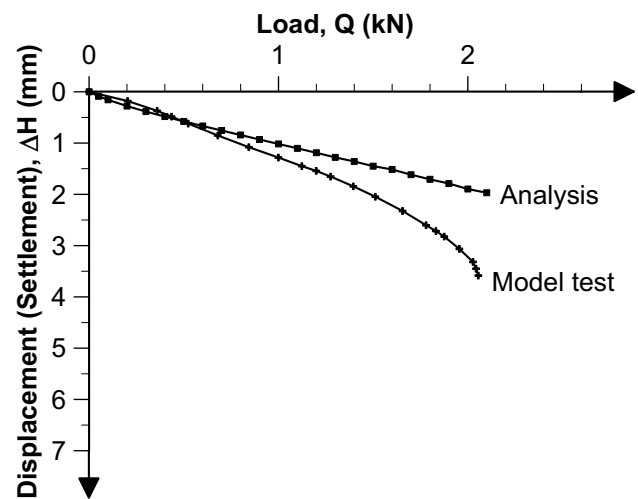

Fig. 6 Load–displacement relation calculated using the analysis and results derived from the conducted model test for the strip footing subjected to central ($e/B = 0$) loading, positioned near unreinforced sand slope
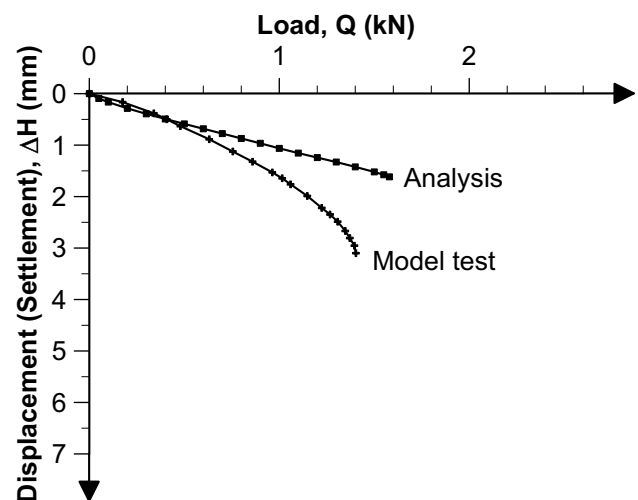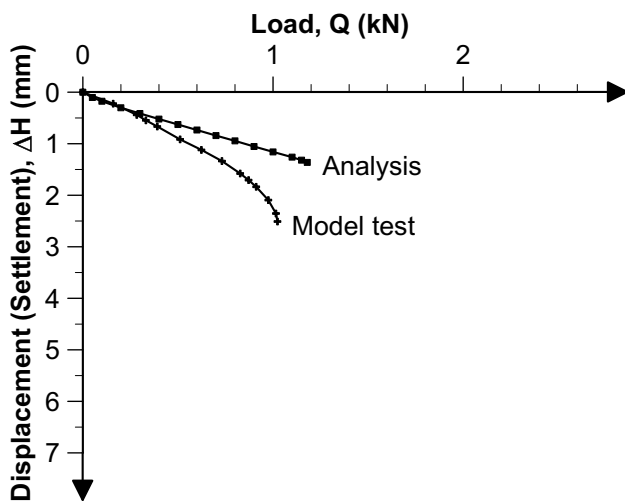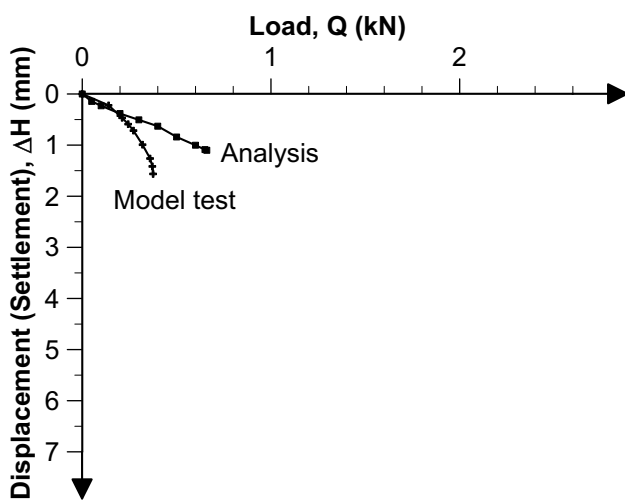

Fig. 7 Load–displacement relation calculated using the analysis and results derived from the conducted model test for the strip footing subjected to eccentrical ($e/B = 1/12$) loading, positioned near unreinforced sand slope

in ultimate loads between the model test and the analysis results are within 5%.

The ultimate loads decreased as the eccentricities increased, which was observed consistently across both the model test and finite element analysis cases. In addition, the values depicting vertical displacement upon reaching failure (ΔH) decreased as eccentricity increased. However, this decrease in the values depicting the vertical displacement upon reaching failure (ΔH) of the model test cases with increasing eccentricities is larger than that of the finite element analysis cases.
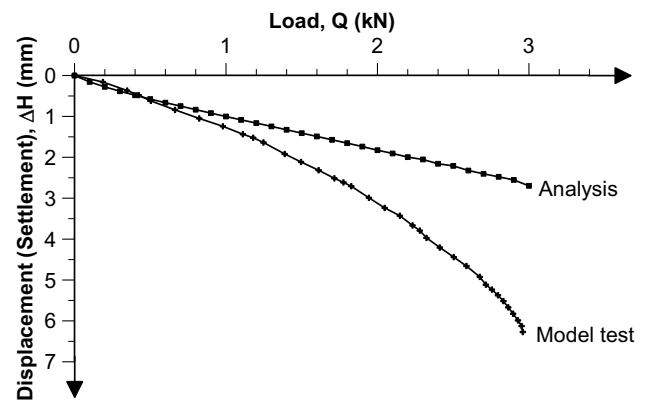
Fig. 8 Load–displacement relation calculated using the analysis and results derived from the conducted model test for the strip footing subjected to eccentrical ($e/B = 1/6$) loading, positioned near unreinforced sand slope
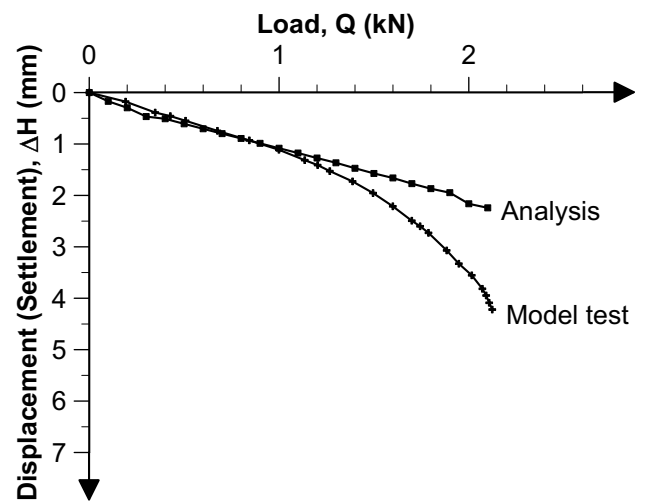

Fig. 9 Load–displacement relation calculated using the analysis and results derived from the conducted model test for the strip footing subjected to eccentrical ($e/B = 1/3$) loading, positioned near unreinforced sand slope

Reinforced case

Figures 10, 11, 12 and 13 present the comparison between the load–displacement relations calculated using finite element analyses and results obtained from the model tests for the strip footing subjected to central and eccentrical loading, positioned near reinforced sand slope. In reinforced cases, there are similar results with unreinforced cases. The utilization of reinforcement led to an increase in the ultimate load in the analysis and the model test.

Fig. 10 Load–displacement relation calculated using the analysis and results derived from the conducted model test for the strip footing subjected to central ($e/B = 0$) loading, positioned near reinforced sand slope
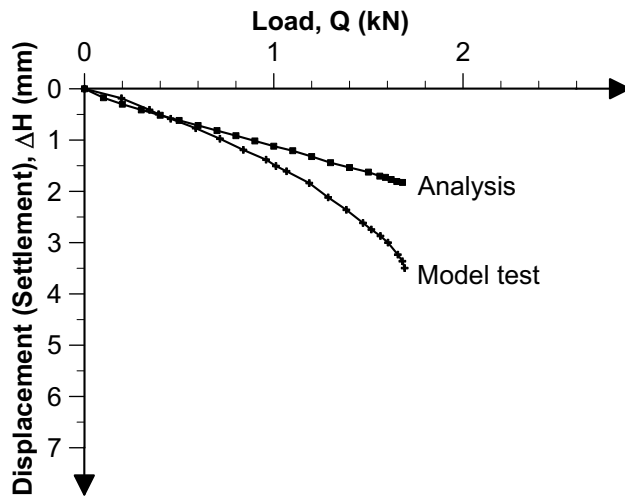

Fig. 11 Load–displacement relation calculated using the analysis and results derived from the conducted model test for the strip footing subjected to eccentrical ($e/B = 1/12$) loading, positioned near reinforced sand slope

The presence of the reinforcement increased both the ultimate load and vertical displacement (ΔH) until soil failure. In other words, the reinforcement enhanced the correlation between the load and displacement. This characteristic remained consistent across all the eccentricity cases.

Conclusions

On the unreinforced and reinforced sand slopes, centrally and eccentrically loaded bearing capacity tests of model strip footing were performed with an experimental design under plane strain (particularly deformation) conditions. The experimental design was likened by using a finite

Fig. 12 Load–displacement relation calculated using the analysis and results derived from the conducted model test for the strip footing subjected to eccentrical ($e/B = 1/6$) loading, positioned near reinforced sand slope
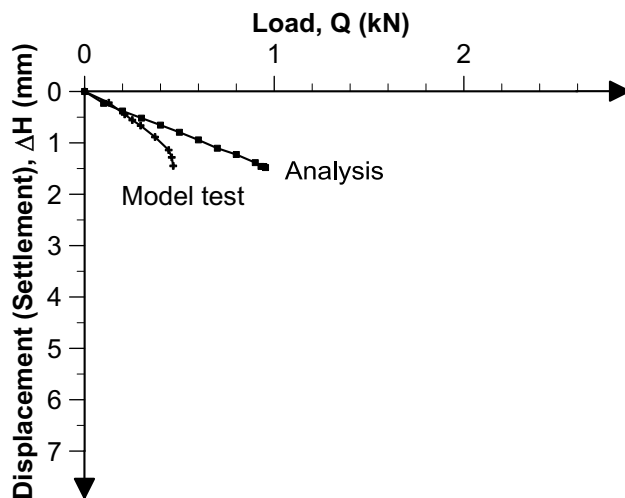
Fig. 13 Load–displacement relation calculated using the analysis and results derived from the conducted model test for the strip footing subjected to eccentrical ($e/B = 1/3$) loading, positioned near reinforced sand slope

element model called ANSYS, and the sand was modeled using an elastic–perfectly plastic material model. The experimental results were compared with the finite element analysis results regarding the ultimate loads and load–displacement behavior. The important findings from the model test results and finite element analyses are as follows:

- The footing model test results on unreinforced and reinforced sand slopes were validated using ANSYS and were in good agreement with the finite element analysis

results regarding load–displacement and general behavior trends.

- It was observed that when the eccentricity increased, the ultimate load decreased in the model test and the finite element analysis cases. In addition, the values depicting the vertical displacement (ΔH) upon reaching failure decreased with increasing eccentricity. However, this decrease in values depicting the vertical displacement (ΔH) upon reaching failure of the model test cases with increasing eccentricities was larger than that of the finite element analysis cases.
- The use of reinforcement increased the ultimate load in both the finite element analysis and the model test. In addition, the reinforcement both increased the ultimate load of the footing and the values depicting vertical displacement (ΔH) upon reaching failure.

Declarations

Conflict of interest The authors declare no competing interests.

References

Abbas JK, Sabbar AS (2011) Finite element analysis for bearing capacity of rectangular footing resting near sloped cohesive soil. Tikrit J Eng Sci 18(3):33–41

Ahad O, Arsam M (2018) Laboratory and numerical modeling of strip footing on geotextile reinforced sand with cement-treated interface. Geotext Geomembr 46:29–39. https://doi.org/10.1016/j.geotexmem.2017.09.003

Ahmadi MH, Asakereh A (2015) Numerical analysis of the bearing capacity of strip footing on reinforced soil slope. Intl Jl of Engineering Trends Technol 29:313–317. https://doi.org/10.14445/22315381/IJETT-V29P258

Alamshahi S, Hataf N (2009) Bearing capacity of strip footings on sand slopes reinforced with geogrid and grid-anchor. Geotext Geomembr 27:217–226. https://doi.org/10.1016/j.geotexmem.2008.11.011

Aliyazicioglu S, Ozturk KF, Gunen MA (2023) Analysis of Gümüşhane-Trabzon highway slope static and dynamic behavior using point cloud data. Advanced LiDAR 3(2):70–75

Al-Jubair HS, Abbas JK (2007) Bearing capacity of eccentrically loaded strip footing near the edge of cohesive slope. Tikrit J Eng Sci 14(2):32–48

Altalhe EB, Taha MR, Abdrabbo FM (2015) Behavior of strip footing on reinforced sand slope. J Civ Eng Manag 21:376–383. https://doi.org/10.3846/13923730.2014.890646

Altalhea EB, Tahaa MR, Abdrabboa FM (2013) Bearing capacity of strip footing on sand slopes reinforced with geotextile and soil nails. Jurnal Teknologi 65(2):1–11

Andrawes KZ, Al-Omari RR, Kirkpatrick WM (1996) Bearing capacity of a strip foundation on a sand layer overlying a smooth rigid stratum. Geotech Geol Eng 14:227–236

ANSYS Basic Analysis Procedure (2005) ANSYS program, Version 10, USA.

ASTM D3080 / D3080M-11 (2011) Standard test method for direct shear test of soils under consolidated drained conditions. American Society for Testing and Materials, West Conshohocken, PA.

ASTM D4253-16 (2016) Standard test methods for maximum index density and unit weight of soils using a vibratory table. American Society for Testing and Materials, West Conshohocken, PA.

ASTM D4254-16 (2016) Standard test methods for minimum index density and unit weight of soils using a vibratory table. American Society for Testing and Materials, West Conshohocken, PA.

ASTM D6913 (2017) Standard test methods for particle-size distribution (gradation) of soils using sieve analysis. American Society for Testing and Materials, West Conshohocken, 34.

ASTM D7181-20 (2020) Standard test method for consolidated drained triaxial compression test for soils. American Society for Testing and Materials, West Conshohocken, PA.

ASTM D854-14 (2006) Standard test methods for specific gravity of soil solids by water pycnometer. American Society for Testing and Materials, West Conshohocken, 8.

Badakhshan E, Noorzad A (2015) Load eccentricity effects on behavior of circular footings reinforced with geogrid sheets. J Rock Mechanics Geotech Eng 7:691–699. https://doi.org/10.1016/j.jrmge.2015.08.006

Bathurst RJ, Blatz JA, Burger MH (2003) Performance of instrumented large-scale unreinforced and reinforced embankments loaded by a strip footing to failure. Can Geotech J 40:1067–1083. https://doi.org/10.1139/T03-052

Binquet J, Lee KL (1975a) Bearing capacity tests on reinforced earth slabs. J Geotech Eng Division, ASCE 101(12):1241–1251

Binquet J, Lee KL (1975b) Bearing capacity analysis of reinforced earth slabs. J Geotech Eng Division, ASCE 101(12):1257–1276

Blatz JA, Bathurst RJ (2003) Limit equilibrium analysis of large-scale unreinforced and reinforced embankments loaded by a strip footing. Can Geotech J 40:1084–1092. https://doi.org/10.1139/T03-053

Briaud JL, Gibbens R (1999) Behaviour of five large scale spread footings in sand. J Geotech Eng Division, ASCE 125(9):787–796

Castelli F, Lentini E (2012) Evaluation of the bearing capacity of footings on slopes. Int J Phys Model Geotechnics 12(3):112–118. https://doi.org/10.1680/ijpmg.14.00038

Castelli F, Motta E (2010) Bearing capacity of strip footings near slopes. J Geotech Geol Eng 28(2):187–198. https://doi.org/10.1007/s10706-009-9277-9

Choudhary AK, Jha JN, Gill KS (2010) Laboratory investigation of bearing capacity behaviour of strip footing on reinforced flyash slope. Geotext Geomembr 28(4):393–402. https://doi.org/10.1016/j.geotexmem.2009.09.007

Chummar AV (1972) Bearing capacity theory from experimental results. J Soil Mechanics Foundations Division, ASCE 98(12):1311–1324

Cornforth DH (1964) Some experiments on the influence of strain conditions on strength of sand. Geotechnique 14:143–167

Cure E, Sadoglu E, Turker E, Uzuner BA (2014) Decrease trends of ultimate loads of eccentrically loaded model strip footings close to a slope. Geomechanics Eng 6(5):469–485. https://doi.org/10.12989/gae.2014.6.5.469

Cure E, Turker E, Uzuner BA (2014b) Analytical and experimental study for ultimate loads of eccentrically loaded model strip footings near a sand slope. Ocean Eng 89:113–118. https://doi.org/10.1016/j.oceaneng.2014.07.018

Dixit MS, Patil KA (2013) Experimental estimate of N_γ values and corresponding settlements for square footings on finite layer of sand. Geomechanics Eng 5(4):363–377. https://doi.org/10.12989/gae.2013.5.4.363

Eastwood W (1955) The bearing capacity of eccentrically loaded foundations on sandy soil. Structural Engineer 29(6):181–187

Huang CC, Tatsuoka F, Sato Y (1994) Failure mechanisms of reinforced sand slopes loaded with a footing. Soils Found 34(2):27–40

Keskin MS, Laman M (2013) Model studies of bearing capacity of strip footing on sand slope. KSCE J Civ Eng 17(4):699–711. https://doi.org/10.1007/s12205-013-0406-x

Khan I, Sharma RK (2023) Bearing capacity evaluation of square footing resting on reinforced sand. J Mining Environ 14(3):813–824. https://doi.org/10.22044/jme.2023.12891.2342

Kirkpatrick WM, Yanikian HA (1975) Side friction in plane strain tests. In: Proceedings of the Fourth South East Conference on Soil Engineering, Kuala Lumpur, Malaysia 76–84.

Ko H, Davidson W (1973) Bearing capacity of footings in plane strain. J SM & FE Division, ASCE 99(1):1–23

Kumar J, Bhoi MK (2008) Interference of multiple strip footings on sand using small scale test. Geotech Geol Eng 26:469–477. https://doi.org/10.1007/s10706-008-9175-6

Lade PV, Lee KL (1976) Engineering properties of soils. Engineering Report, UCLA-ENG-7652, Los Angeles, CA, 145.

Laman M, Yıldız L, Keskin MS, Uncuoglu E (2007) Experimental investigation of strip footing on reinforced sand slope. IMO Teknik Dergi (in Turkish) 4197–4217.

Lau CK, Bolton MD (2011) The bearing capacity of footings on granular soils I: Numerical analysis. Geotechnique 61(8):627–638. https://doi.org/10.1680/geot.7.00206

Lee KM, Manjunath VR (2000) Experimental and numerical studies of geosynthetic-reinforced sand slopes loaded with a footing. Can Geotech J 37(4):828–842. https://doi.org/10.1139/t00-016

Luo Z, Ding X, Ou Q, Fang H (2023) Bearing capacity and deformation behavior of rigid strip footings on coral sand slopes. Ocean Eng 267:113317. https://doi.org/10.1016/j.oceaneng.2022.113317

Mase LZ, Putri MA, Edriani AF, Lai VQ, Keawsawasvong S (2023) Prediction of the bearing capacity of strip footing at the homogenous sandy slope based on the finite element method and multivariate adaptive regression spline. Transportation Infrastructure Geotechnol. https://doi.org/10.1007/s40515-023-00334-x

Mehdipour I, Ghazavi M, Moayed RZ (2013) Numerical study on stability analysis of geocell reinforced slopes by considering the bending effect. Geotext Geomembr 37:23–34. https://doi.org/10.1016/j.geotexmem.2013.01.001

Munawir A, Dewi SM, Soehardjono A, Zaika Y (2013) Bearing capacity of continuous footing on slope modeling with composite bamboo pile reinforcement. Int J Curr Eng Technol 3(2):557–562. https://doi.org/10.1016/j.geotexmem.2013.01.001

Nova R, Montrasio L (1991) Settlements of shallow foundations on sand. Geotechnique 41(2):243–256

Pfeifle TW, Das BM (1979) Model tests for bearing capacity in sand. J Geotech Eng Division, ASCE 105(9):1112–1116

Sawwaf MA (2007) Behavior of strip footing on geogrid-reinforced sand over a soft clay slope. Geotext Geomembr 25:50–60. https://doi.org/10.1016/j.geotexmem.2006.06.001

Selvadurai APS, Gnanendran CT (1989) An experimental study of a footing located on a sloped fill: influence of a soil reinforcement layer. Can Geotech J 26(3):467–473

Taha MR, Altalhe EB (2013) Numerical and experimental evaluation of bearing capacity factor $N\gamma$ of strip footing on sand slopes. Int J Phys Sci 8(36):1807–1823. https://doi.org/10.5897/IJPS2013.4000

Taiebat HA, Carter JP (2000) Numerical studies of the bearing capacity of shallow foundations on cohesive soil subjected to combined loading. Geotechnique 50:409–418. https://doi.org/10.1680/geot.2000.50.4.409

Thanapalasingam J, Gnanendran CT (2008) Predicting the performance of foundations near reinforced sloped fills. The 12th International Conference of International Association for Computer Methods and Advances in Geomechanics, (IACMAG) 3727–3734.

Turker E, Sadoglu E, Cure E, Uzuner BA (2014) Bearing capacity of eccentrically loaded strip footings close to geotextile-reinforced

sand slope. Can Geotech J 51:884–895. https://doi.org/10.1139/cgj-2014-0055

Xiao Y, Zhao MH, Zhang R, Zhao H, Wu GQ (2019) Undrained bearing capacity of strip footings placed adjacent to two-layered slopes. Int J GeoMech 19(8):06019014. https://doi.org/10.1177/8755293020957332

Yang SC, Leshchinsky B, Cui K, Zhang F, Gao YF (2021) Influence of failure mechanism on seismic bearing capacity factors for shallow foundations near slopes. Geotechnique 71(7):594–607. https://doi.org/10.1680/jgeot.19.P.329

Yoo C (2001) Laboratory investigation of bearing capacity behavior of strip footing on geogrid-reinforced sand slope. Geotext Geomembr 19(5):279–298

Yu Y, Damians IP, Bathurst RJ (2015) Influence of choice of FLAC and PLAXIS interface models on reinforced soil-structure interactions. Computers Geotechniques 65(2):164–174. https://doi.org/10.1016/j.compgeo.2014.12.009